

Radial wave thermoacoustic engines: Theory and examples for refrigerators and high-gain narrow-bandwidth photoacoustic spectrometers

W. Patrick Arnott^{a)}

Atmospheric Science Center, Desert Research Institute, P.O. Box 60220, Reno, Nevada 89506

Jay A. Lightfoot and Richard Raspet

Physics Department, University of Mississippi, University, Mississippi 38677

Hans Moosmüller

Energy and Environmental Engineering Center, Desert Research Institute, P.O. Box 60220, Reno, Nevada 89506

(Received 20 January 1995; revised 1 September 1995; accepted 5 September 1995)

A theoretical analysis of radial wave thermoacoustic engines in cylindrical resonators is developed. Impedance and pressure translation equations are presented for open sections of the resonator and for heat exchangers. Coupled first-order differential equations are given for pressure and impedance in the temperature gradient supporting engine section (stack). These quantities are used to calculate heat and work flows and to predict engine performance. Theory and design of a variable quality factor resonator for enhanced photoacoustic spectroscopy are presented. The short stack approximation is developed for the radial geometry and is used along with plane-wave equations to compare refrigerator performance for these two geometries. Results of the comparison are that engines in the plane-wave geometry are better overall refrigerators when maximizing the coefficient of performance and cooling capacity together. © 1996 Acoustical Society of America.

PACS numbers: 43.28.Fp, 43.35.Ud, 43.58.Bh

LIST OF SYMBOLS

A_{res}	resonator area in cross section	T_a, T_b	radial stack ambient temperatures at r_a, r_b
a	resonator radius	T_0	ambient temperature
C_m	coefficient of compromise	T_1	acoustic, i.e., excess temperature
COP	coefficient of performance	T_{0r}	radial wave stack temperature gradient
COP_c	Carnot coefficient of performance	T_{0z}	plane-wave stack temperature gradient
c	sound speed	V_G	ambient volume of gas in the stack
c_p	isobaric heat capacity per unit mass	v_s	standing-wave particle velocity
d	thermoacoustic element length	\bar{W}_2	work flow
F	thermoviscous dissipation function	Z	specific acoustic impedance
f_0	resonance frequency	Z_{bl}	boundary layer specific acoustic impedance
$H_n^{(k)}$	Hankel function of order n and type k	Z_{int}	intrinsic impedance
h	resonator axial length	z	axial coordinate
Im	imaginary part of	α	function used in stack impedance equation
J_n	Bessel function of order n	β	coefficient of thermal expansion
k	acoustic propagation constant	γ	ratio, isobaric to isochoric specific heats
k_0	adiabatic acoustics propagation constant	Γ	Swift's normalized temperature gradient
m	COP/COP_c preference exponent	Δf	photoacoustic spectrometer bandwidth
N_{pr}	Prandtl number	δ_κ	thermal penetration depth
P_0	ambient pressure	δ_ν	viscous penetration depth
P_1	acoustic pressure	ϵ	dummy variable
Q	quality factor of resonance	ϵ_s	Swift's plate heat capacity ratio
\bar{Q}_2	heat flow	ϕ	normalized stack location
R	twice pore or resonator cross sectional area divided by pore perimeter	η	dynamic viscosity
r	radial coordinate	κ	thermal conductivity
r_a, r_b	inner and outer radial stack radii: $r_b = r_a + d$	λ	shear wave number = $\sqrt{2}R/\delta_\nu$
		λ_T	thermal disturbance number = $\sqrt{2}R/\delta_\kappa$
		ρ_0	ambient gas density
		ρ_1	acoustic gas density
		τ	normalized stack temperature gradient

^{a)}W. Patrick Arnott is an Adjunct Assistant Professor in the Department of Physics, University of Mississippi.

τ_{\max}	maximum refrigerator stack normalized temperature gradient
Ω	stack or heat exchanger porosity
ω	radian frequency

ω_c	complex eigenfrequency
ξ_s	standing-wave particle displacement
ζ	stack or heat exchanger thickness
*	complex conjugation operator

INTRODUCTION

Thermoacoustic heat engines involve heat transfer between a solid and a fluid undergoing compression, expansion, and displacement. A comprehensive review is available¹ as is a review of the foundation work for modern thermoacoustics.² Most previous work considered placing thermoacoustic engines in plane-wave resonators. A framework for analyzing and predicting the performance of engines in radial wave resonators is given in this paper.

Swift¹ briefly considered thermoacoustic engines in cylindrical resonators with only the lowest radial mode active. He developed the wave equation, discussed how to calculate energy flux, and showed a possible conceptual arrangement for a working engine. We advance upon Swift's work by establishing pressure and impedance translation equations for all points within the resonator. These equations are useful for computing acoustical quantities in open sections of the resonator, in heat exchangers, and in the temperature-gradient-supporting sections known as thermoacoustic engines. These relations naturally connect the various sections and give an explicit prescription for computing properties of complicated resonators containing several engines. This development parallels the previous analysis of engines in plane-wave resonators.³

A conceptual design of a radial wave thermoacoustic engine is shown in Fig. 1. A cylindrical resonator is filled with a gas such as helium. The nominal pressure distribution is a radial or breathing mode. Thermoacoustic engines may be placed at either or both locations shown in Fig. 1 and are made of material with low thermal conductivity to support a temperature gradient. Since some of the first thermoacoustic engines were produced by stacking parallel plates, thermoacoustic engines are also referred to as stacks. The thermoacoustic elements are between pressure nodes and antinodes so that the product of acoustic pressure and particle velocity is significant. It is this product that is important for thermoacoustic transport of heat up to the temperature gradient in the refrigerator application or, in the sound source application, for producing net acoustic power when the applied temperature gradient is sufficiently large.¹⁻⁴ Heat exchangers made of material with high thermal conductivity are on both sides of the engine and are used to transfer heat between outside sources and sinks. Heat exchangers nearest the pressure antinodes are at higher temperatures than heat exchangers facing the pressure node. A full system would have many of the annuli shown in Fig. 1. The annuli would be stacked perpendicular to the plane of the figure with a spacing between adjacent annuli of about one to two thermal penetration depths in the gas. The system can be operated as a sound source when high-temperature gradients are applied across the engines, as refrigerators when driven by an external

acoustic source, or as a combination of both, just as with plane-wave engines.¹

Particle velocity and pressure distributions in empty resonators are of course different for radial and plane-wave modes. For gas parcels in a standing wave, displacement and acoustic pressure are in phase which gives rise to a temperature gradient through the relation of pressure and temperature. The temperature increase during compression of a gas parcel undergoing displacement in a standing wave is followed by a temperature decrease during expansion half a cycle later when the gas parcel is displaced in the opposite direction. This standing-wave temperature gradient is useful to compare with temperature gradients applied to or developed on the stack.¹ For example in the inviscid limit where the Prandtl number $N_{pr}=0$, the stack will operate as a refrigerator when its developed temperature gradient is less than the standing-wave gradient and as a prime mover when its applied temperature gradient is larger than the standing-wave gradient. The temperature gradients associated with standing waves in empty plane and radial resonators are considered to gain familiarity with some differences between plane- and radial wave geometries. Swift¹ refers to this as the critical mean-temperature gradient, ∇T_{crit} . The coordinate system and possible stack locations for radial and plane engines are shown schematically in Fig. 2(a) and (b). The critical temperature gradients are

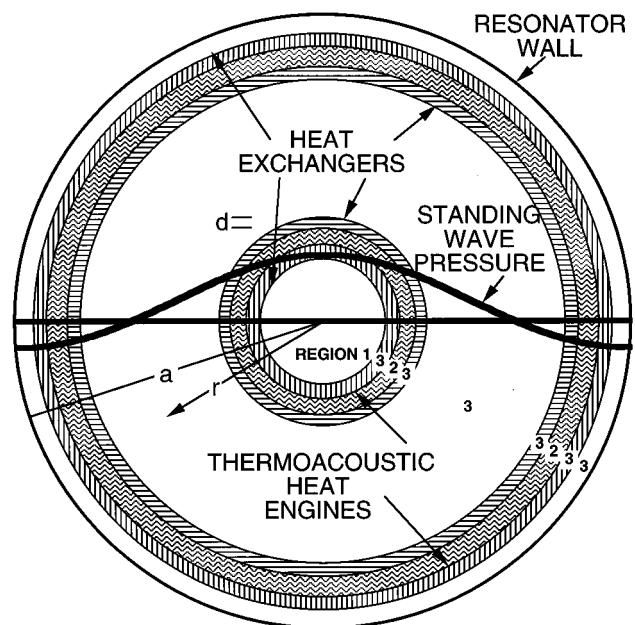


FIG. 1. Possible arrangements for a radial wave thermoacoustic engines. Cold heat exchangers face the pressure nodes. The three regions used in analysis are shown. The z axis (not shown) is perpendicular to the plane of the paper. Distance d is shown as the cold heat exchanger length and is generally used to represent the length of any thermoacoustic element.

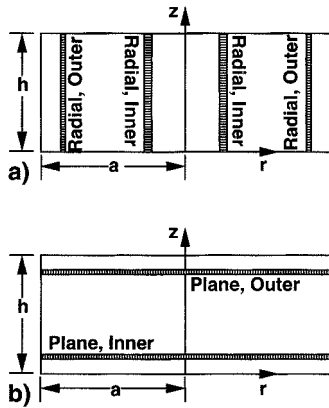


FIG. 2. Coordinate system and stack locations (e.g., radial inner, etc.) for (a) radial and (b) plane-wave resonators. Resonator height is h and radius is a . Particle velocity is in the r direction in (a) and is in the z direction in (b).

$$\frac{a\beta T_{0r,c}}{\gamma-1} = -3.832 \frac{J_0(3.832r/a)}{J_1(3.832r/a)}, \quad (1a)$$

$$\frac{h\beta T_{0z,c}}{\gamma-1} = -\pi \frac{\cos(\pi z/h)}{\sin(\pi z/h)}, \quad (1b)$$

where $T_{0r,c}$ and $T_{0z,c}$ are the critical mean-temperature gradients associated with radial and plane waves, respectively.

Figure 3 shows the critical temperature gradients. In the inviscid approximation, engines act as refrigerators when the ambient temperature gradient on the stack is in the region between the curves and zero temperature gradient line; otherwise, engines are prime movers (sound sources). For example, radial and plane stacks at $z/h=r/a=0.8$ and normalized stack temperature gradients of 10 would be prime movers, while radial and plane stacks at $z/h=r/a=0.2$ and normalized stack temperature gradients of -1 would be refrigerators, in this approximation. The curves cross the zero temperature gradient line at pressure nodes. The pressure node for the radial case occurs at $r/a \approx 0.63$. Some qualitative conclusions are that radial refrigerators with stacks between $0 < r/a < 0.628$ can achieve larger temperature gradients than plane-wave refrigerators, and that radial prime movers with stacks between $0.628 < r/a < 1$ will operate at

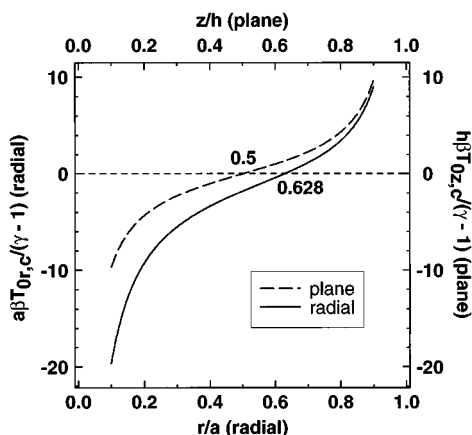


FIG. 3. Dimensionless critical temperature gradient for plane (dashed line) and radial wave engines (full line).

lower temperature gradients than either plane-wave prime movers or the radial prime mover near the center of the resonator.

This paper is organized as follows. Section I and its subsections contain the formal solution for the first-order acoustic properties of pressure, specific acoustic impedance, and the second-order enthalpy flow. Section I C is an application of the general theory which serves the dual purpose of teaching the calculation techniques and of demonstrating an interesting dependence of resonance frequency on stack plate spacing. The application has relevance to design of thermoacoustically enhanced photoacoustic spectrometers.⁵ The short stack approximation similar to that given for plane waves³ (not limited by the additional boundary layer approximation¹) is presented in Sec. II, and is used in its subsections to compare the performance of plane and radial wave refrigerators.

I. RADIAL WAVE ANALYSIS

A system of equations is established for computing pressure, specific acoustic impedance, and enthalpy flow at all points. Enthalpy flow can be evaluated when pressure and impedance are known, and is needed for estimation of the engine efficiency and power. The analysis closely parallels that given for plane-wave systems³ and for that reason the treatment here is brief.

Figure 2(a) and (b) shows the coordinate system. Analysis proceeds by breaking the engine up into the three types of regions, shown schematically in Fig. 1, for the purpose of isolating elements that can be evaluated by the same type of equations and that have similar acoustic properties. Region 1 contains the resonator center where, by symmetry, a pressure antinode and particle velocity node exist. Region 2 is the thermoacoustic engine and will also interchangeably be referred to as the stack in this paper. The stack usually has a radial temperature gradient. Region 3 is associated with resonator and heat exchanger sections. Specific acoustic impedance and pressure translation theorems are derived for analyzing wave propagation in region 3 thermoacoustic elements. These equations are analogous to Rayleigh's impedance translation theorem for plane waves.^{3,6} Analyses for electromagnetic waves in radially symmetric layered media,⁷ and of radial acoustic waves in ducts with finite impedance walls,⁸ have features similar to the approach taken here in the analysis of regions 1 and 3.

The basic set of equations used by Rott² for analyzing plane-wave engines can be altered for use in analyzing radial wave engines.¹ The radian frequency ω is used with the $\exp(-i\omega t)$ convention. Density is generally given by ρ , pressure by P , radial and longitudinal particle velocity by v and v_z , and temperature by T . Subscripts zero and one correspond to ambient and first-order (acoustic) quantities, respectively. All components of particle velocity and the excess temperature T_1 are taken to be zero at the fluid-solid boundary. The excess temperature boundary condition is appropriate when the product of stack density, heat capacity per unit mass, and thermal conductivity is much greater than the same product for the working fluid, and when the stack plate thickness is much greater than the thermal penetration depth

in the solid material of the stack.¹ Both criteria for using the zero excess temperature boundary condition are usually satisfied in practice when the working fluid is a gas at moderate pressure. This boundary condition is the $\epsilon_s \rightarrow 0$ limit of the equations in Ref. 1.

A. Specific acoustic impedance and pressure translation theorems, and enthalpy flow

Counterpropagating radial waves having different complex amplitudes may be superimposed to describe wave propagation in open resonator and heat exchanger sections. Boundary conditions at interfaces are continuity of acoustic pressure and continuity of specific acoustic impedance. However, in the stack sections where the ambient temperature depends on position, coupled first-order differential equations are used to determine acoustic pressure, specific acoustic impedance, and in some instances the ambient temperature.

Denote by $Z(r)$ the specific acoustic impedance at position r , where $Z(r)$ is the acoustic pressure divided by the radial particle velocity. The intrinsic or characteristic impedance of a section of resonator, heat exchanger, or stack is given by

$$Z_{\text{int}} = \frac{\rho_0 \omega}{\Omega F(\lambda) k}, \quad (2)$$

where $\Omega = R/(\zeta + R)$ is the porosity, R is the plate spacing, and ζ is plate thickness. The thermoviscous dissipation function, $F(\epsilon)$, for the parallel-plate geometry is^{1,3,9}

$$F(\epsilon) = 1 - \frac{2}{\epsilon \sqrt{-i}} \tanh\left(\frac{\epsilon \sqrt{-i}}{2}\right). \quad (3)$$

The dummy variable $\epsilon = \lambda_T$ when thermal dissipation is considered, and $\epsilon = \lambda$ for viscous dissipation. Other parameters are the Prandtl number $N_{\text{pr}} = \eta c_p / \kappa$, $\lambda = (\rho_0 \omega / \eta)^{1/2} R$, and $\lambda_T = \lambda N_{\text{pr}}^{1/2}$. The quantity R is the spacing between heat exchanger annuli, or the distance between the top and bottom plates [h in Fig. 2(a)] for open sections of the resonator. The acoustic propagation constant k is given by

$$k^2 = \frac{\omega^2}{c^2} \frac{\gamma - (\gamma - 1) F(\lambda_T)}{F(\lambda)}, \quad (4)$$

where c is the adiabatic sound speed.

Determined first are the acoustic pressure and specific acoustic impedance in the resonator and heat exchanger sections shown as region 3 in Fig. 1. These quantities at position $r - d$ can be determined through use of pressure and impedance translation equations which use given values of these quantities at position r . Using a procedure similar to that outlined in Ref. 3, the translation equation for pressure is

$$\begin{aligned} P_1(r-d) = & P_1(r) \frac{\pi k r i}{4} \left(H_1^{(1)}[kr] H_0^{(2)}[k(r-d)] \right. \\ & - H_1^{(2)}[kr] H_0^{(1)}[k(r-d)] - i \frac{Z_{\text{int}}}{Z(r)} \\ & \times (H_0^{(2)}[kr] H_0^{(1)}[k(r-d)] - H_0^{(1)}[kr] \\ & \left. \times H_0^{(2)}[k(r-d)]) \right). \quad (5) \end{aligned}$$

The translation equation for specific acoustic impedance is

$$\begin{aligned} Z(r-d) = & Z_{\text{int}} \{ Z(r) (H_1^{(1)}[kr] H_0^{(2)}[k(r-d)] \\ & - H_1^{(2)}[kr] H_0^{(1)}[k(r-d)]) - i Z_{\text{int}} (H_0^{(2)}[kr] \\ & \times H_0^{(1)}[k(r-d)] - H_0^{(1)}[kr] H_0^{(2)}[k(r-d)]) \} / \\ & \{ Z_{\text{int}} (H_1^{(1)}[k(r-d)] H_0^{(2)}[kr] \\ & - H_1^{(2)}[k(r-d)] H_0^{(1)}[kr]) - i Z(r) (H_1^{(1)}[k(r-d)] \\ & \times H_1^{(2)}[kr] - H_1^{(2)}[k(r-d)] H_1^{(1)}[kr]) \}. \quad (6) \end{aligned}$$

Hankel functions $H_m^{(j)}[x]$ of order m , type j , and argument x are used in Eqs. (5) and (6). It can be shown using the asymptotic expansion for Hankel functions with $x \gg 1$,

$$H_n^{(1)}(x) \approx (2/\pi x)^{1/2} \exp[i(x - n\pi/2 - \pi/4)]$$

and

$$H_n^{(2)}(x) \approx (2/\pi x)^{1/2} \exp[-i(x - n\pi/2 - \pi/4)],$$

that Eqs. (5) and (6) reduce to the one-dimensional plane-wave forms given by Eqs. (36) and (37) in Ref. 3.

Specific acoustic impedance and acoustic pressure are determined in the stack, region 2 in Fig. 1, as follows:

$$\frac{dZ(r)}{dr} = ik(r) Z_{\text{int}}(r) \left(1 - \frac{Z(r)^2}{Z_{\text{int}}(r)^2} \right) + \left(2\alpha(r) + \frac{1}{r} \right) Z(r) \quad (7)$$

and

$$\frac{dP_1(r)}{dr} = ik(r) Z_{\text{int}}(r) \frac{P_1(r)}{Z(r)}, \quad (8)$$

where $\alpha(r)$ is given by

$$\alpha(r) = \frac{\beta T_{0r}}{2} \frac{F(\lambda_T)/F(\lambda) - 1}{1 - N_{\text{pr}}}. \quad (9)$$

The temperature gradient along the plate in the radial direction is given by $T_{0r} = \partial T_0(r) / \partial r$. All parameters such as α and k are dependent on r since the ambient temperature generally depends on r in the stack. Except for the term involving $1/r$ in Eq. (7), Eqs. (7) and (8) are the same as their plane-wave counterparts given by Eqs. (33) and (35) in Ref. 3.

The expressions for heat, work, and enthalpy flows for the radial wave geometry are the same as the plane-wave geometry equations.¹ Expressions for heat, and work flows, are given in terms of acoustic pressure and specific acoustic impedance in Ref. 3. For the radial wave geometry, it is important to note the dependence of enthalpy flow on the

cross-sectional area of the resonator as $A_{\text{res}}(r) = 2\pi rh$. By contrast, the plane-wave geometry has $A_{\text{res}} = \pi a^2$.

B. Numerical implementation of the theory

Recent theoretical and experimental work has considered the effect of stack temperature gradient on the resonator quality factor Q , and resonance frequency f_0 .^{4,10-13} The quantity $1/Q$ is the dissipated acoustic power per radian frequency per stored acoustic energy throughout the entire resonator. Although acoustic power is normally absorbed through the processes of heat conduction and viscous dissipation at interfaces between solids and fluids, a stack with an appropriate temperature gradient can generate acoustic power.^{4,12} Resonance frequency is determined by thermoacoustic element lengths and dispersion caused by narrow plate spacing. Both Q and f_0 can be incorporated into a single quantity, the complex eigenfrequency $\omega_c = 2\pi f_0 - i\pi f_0/Q$, which describes the temporal response throughout the resonator of an excited resonance at $t=0$, $P_1(t)/P_1(0) = \exp(-i\omega_c t)$. The complex eigenfrequency of a radial wave prime mover below the onset of self-oscillation will be computed to illustrate the appropriate technique for the radial geometry, and to point out the dependence of f_0 and Q on stack plate spacing.

When determining the quality factor or onset temperature for plane-wave systems, it is usually sufficient to consider a constant temperature gradient in the stack.^{4,12} For the radial geometry, however, because a constant amount of heat is spread into an increasing area as r increases, the ambient temperature gradient is given by

$$T_{0r}(r) = T_{0z} \frac{d}{r} \frac{1}{\ln(1+d/r_a)}, \quad (10)$$

where $d = (r_b - r_a)$ is the stack length, r_a and r_b are the inner and outer radius of the stack, and $T_{0z} = (T_b - T_a)/(r_b - r_a)$ is the temperature gradient used for the plane geometry. Note that $T_{0r}(r) \approx T_{0z}$ when $d \ll r_a$ as is the case in the short stack approximation below, and when $r_a \rightarrow \infty$ which approximates the plane geometry.

The complex eigenfrequency can be determined by numerically searching for values of f_0 and Q that give the same result for the calculated impedance looking to the right at some position, with that computed looking to the left.⁴ Consider the resonator region 1 in Fig. 1. By symmetry, a particle velocity node must occur at the resonator center, yielding an expression for the acoustic pressure,

$$P_1(r) = P_1(0)J_0(kr), \quad (11)$$

and for the specific acoustic impedance,

$$Z(r) = -iZ_{\text{int}} \frac{J_0(kr)}{J_1(kr)}. \quad (12)$$

Equations (11) and (12) can be obtained by using $r \rightarrow 0$, $d \rightarrow -r$ and $Z(0) \rightarrow \infty$ in Eqs. (5) and (6), respectively, so region 1 in Fig. 1 can be regarded as a special case of region 3. The acoustic propagation constant k is from Eq. (4), and the intrinsic or characteristic impedance is from Eq. (2) with $\Omega=1$. Note that even though $i = \sqrt{-1}$ occurs in Eq. (12), impedance is not purely imaginary because of the acoustic

propagation constant k . In other words, $Z(r)$ in region 1 must still reflect the fact that thermal and viscous dissipation occurs at the resonator walls. Define Z_- as the specific acoustic impedance at the inside boundary of the heat exchanger that faces the resonator center, where Z_- is computed from Eq. (12) using the appropriate inner radius of this heat exchanger. It is now necessary to substitute ω_c for ω in Eqs. (5), (6), and Eq. (12) since the complex eigenfrequency of the system is desired.

Here, Z_- is stored as the impedance looking toward the resonator center from the inner radius of the heat exchanger. Eventually Z_- must be compared with Z_+ , where Z_+ is the impedance at the same location, but looking toward the resonator wall. To compute Z_+ , begin at the resonator wall where impedance is much greater than the characteristic impedance $\rho_0 c$, but is finite because thermal dissipation occurs during the acoustic cycle as the gas undergoing compression and expansion exchanges heat with the wall. The boundary layer impedance, denoted by Z_{bl} , for the cylinder wall can be shown to be¹⁴

$$\begin{aligned} Z_{\text{bl}} &= -\frac{\rho_0 c^2}{\gamma-1} \sqrt{\frac{\rho_0 c_p}{i\omega\kappa}} \frac{J_0[(1+i)a/\delta_\kappa]}{J_1[(1+i)a/\delta_\kappa]} \\ &\approx \frac{\rho_0 c^2}{\gamma-1} \sqrt{\frac{i\rho_0 c_p}{\omega\kappa}}, \quad \text{for } a \gg \delta_\kappa. \end{aligned} \quad (13)$$

In Eq. (13) $\delta_\kappa = \sqrt{2\kappa/\rho_0\omega c_p}$ is the thermal boundary layer thickness (i.e., the distance heat can diffuse during time $1/\omega$), and the second approximate form is just the expression for boundary layer impedance when the wall is flat.^{6,14} In thermoacoustics the second form of Z_{bl} is applicable since $a \gg \delta_\kappa$.

Having established Z_{bl} , impedance at the outer radius of the outer heat exchanger is computed using Z_{bl} and Eq. (6). This value of impedance is used again with Eq. (6) to compute impedance at the outer radius of the stack (region 2 in Fig. 1), though this time with k and Z_{int} appropriate for the heat exchanger and with d the heat exchanger length. Using Eq. (7) and the computed impedance at the outer stack border as the boundary condition, numerical integration of the differential equation yields the impedance at the inner stack border. Finally, Eq. (6) is used again to translate impedance from the inner stack boundary to the inner boundary of the inner heat exchanger. Denote this value of impedance as Z_+ . If it is found that $Z_- = Z_+$, then the current choice of ω_c is the complex eigenfrequency; otherwise, the entire procedure must be repeated with another trial value of ω_c . Note that both the real and imaginary parts of impedance must be matched by adjusting both the real and imaginary parts of ω_c , which is equivalent to adjusting f_0 and Q .

It should be noted that this procedure can be used to compute $Q < 0$ (i.e., exponential increase rather than decrease of acoustic pressure in the resonator) that occurs for a superheated prime mover for a short time after Q spoiling ceases.¹³ When a prime mover goes into onset, the resonator has become unstable with respect to acoustic oscillations, and $Q \rightarrow \infty$. The eigenfrequency is real in this case and is given simply by $\omega_c = 2\pi f_0$. Stability curves for the prime mover^{4,11} can be computed by adjusting values of f_0 and T_{0z}

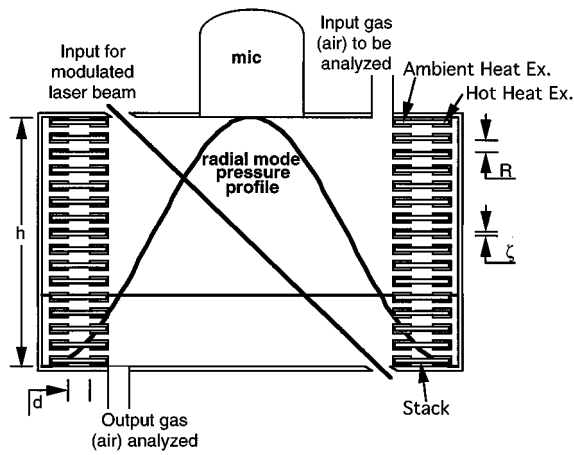


FIG. 4. Conceptual design of a thermoacoustic enhanced photoacoustic spectrometer.

until impedance is matched. Different resonator modes can be studied by choosing appropriate starting values of f_0 .

C. Design of a thermoacoustic enhanced photoacoustic spectrometer

The example calculation for resonance frequency and Q of a radial prime mover considers the outer stack location. Specific dimensions will be used in describing the resonator, heat exchangers, and stack. Resonator overall dimensions are similar to those reported in photoacoustic spectroscopy measurements made using empty resonators^{15,16} (no thermoacoustic elements). Refer to Fig. 4. A laser beam modulated at the acoustic resonance frequency passes through the resonator to couple energy into a particular resonator mode when light is absorbed by aerosols and/or particular gaseous species.^{15,16} The acoustic signal is proportional, among others, to the laser power, to the absorption coefficient of the gaseous species or aerosol (hence the connection with spectroscopy), and to the resonator Q . Thermoacoustics offers the possibility of adjusting Q by controlling the temperature gradient of the stack. Resonator Q increases with the applied temperature gradient when the hot end of the stack faces a pressure antinode and decreases when the hot end faces a pressure node. It can be shown that when the acoustic noise in the resonator is Gaussian with a wide spectrum, and when the bandwidth of the microphone detection electronics is much greater than the resonator bandwidth, the signal-to-noise ratio for the measurement scales as $Q^{1/2}$. The $Q^{1/2}$ dependence of the signal to noise ratio can be qualitatively understood as follows: Signal and noise are both enhanced by Q ; however, the noise amplitude bandwidth is proportional to $(f_0/Q)^{1/2}$. Hence it is desirable to perform photoacoustic spectroscopy with high Q resonators. A thermoacoustic enhanced resonator can be described as an analog amplifier with adjustable gain Q for frequency f_0 , with adjustable bandwidth $\Delta f = f_0/Q$, and with discrimination¹⁷ of signal against acoustic broadband noise of $Q^{1/2}$.

Refer to Fig. 4. System dimensions are specified starting at the resonator center. The inner portion of the resonator, the ambient heat exchanger, and the inner radius of the stack all are assumed to be at an ambient temperature $T_a = 293$ K. The

quantity T_{0z} in Eq. (10) will be held at a constant value $T_{0z} = 26.6$ K/mm. The resonator height h is taken as 5 cm. The distance from resonator center to the ambient heat exchanger is 8.98 cm. The cold heat exchanger is 1.08 mm long. Three stack lengths are considered: $d = 3.28$ mm, $0.8d$, and $1.2d$. The quantity R denotes both the stack and heat exchangers plate spacings, and will vary in the calculation. The plates thus become thicker as R increases since the calculation is for constant stack and heat exchanger porosity $\Omega = 0.7$. The hot heat exchanger is 1.15 mm long. The section from the hot heat exchanger to the outer diameter of the resonator is 9.98 mm long, and its temperature is $T_b = 380.2$ K for $d = 3.28$ mm, is $T_b = 362.8$ K for $0.8d$, and is $T_b = 397.7$ K for $1.2d$. The working fluid is taken as dry air with ambient pressure $P_0 = 100$ kPa. For comparative purposes the resonance frequency and Q were computed for both an empty resonator having diameter 21.06 cm, and for the above thermoacoustic arrangement when $T_{0z} = T_{0r}(r) = 0$.

Figure 5(a) and (b) shows the resonance frequency, f_0 , and Q as a function of stack and heat exchanger plate spacing R . The empty resonator has $f_0 \approx 1984$ Hz and $Q \approx 550$. The case of no stack temperature gradient and Fig. 5(a) will be considered first. Starting at largest R , f_0 decreases as R decreases because the phase velocity in stack and heat exchangers also decreases. Now as $R \rightarrow 0$, f_0 increases since the attenuation of sound in the stack and heat exchangers is quite severe, and the characteristic impedance of these elements $\rightarrow \infty$. Hence the cold heat exchanger begins to approximate a nearly rigid termination and f_0 is approximately determined using the distance from the resonator center to the cold heat exchanger and the ambient sound speed. The minimum f_0 occurs as a trade-off of these dependences on R . In Fig. 5(b) Q increases with R for no temperature gradient because the thermal and viscous boundary layers become smaller in relation to the plate spacing so the attendant losses decrease. Note that Q also increases as $R \rightarrow 0$ because the cold heat exchanger better approximates a rigid termination in this limit.

A fundamentally different dependence for Q occurs when the stack has a sufficiently large temperature gradient. Q increases by as much as a factor of 2 over the empty resonator value for a stack plate spacing of $R \approx 0.21$ mm. The thermal disturbance number at the hot end corresponding to this value of R and the stack with length $1.2d$ is $\lambda_T \approx 3.81$, which gives $R/\delta_\kappa \approx 2.7$. Gas within $\approx 1.35 \delta_\kappa$ of the stack walls receives some acoustic power gain due to the temperature gradient in addition to the normal viscous and thermal losses present with no temperature gradient.⁴ This result again¹⁻⁴ demonstrates that the important length scale for optimal thermoacoustic performance is δ_κ . The stack is longest for the thickest line in Fig. 5(a) and (b), which produces the greatest thermoacoustic gain (i.e., highest Q) since, as shown in the short stack approximation below, acoustic power production and dissipation in the stack are proportional to stack length. As R increases beyond the value for maximal Q , the volume of gas receiving thermoacoustic gain decreases as does Q . For $R \rightarrow 0$, Q decreases since the gas begins to take

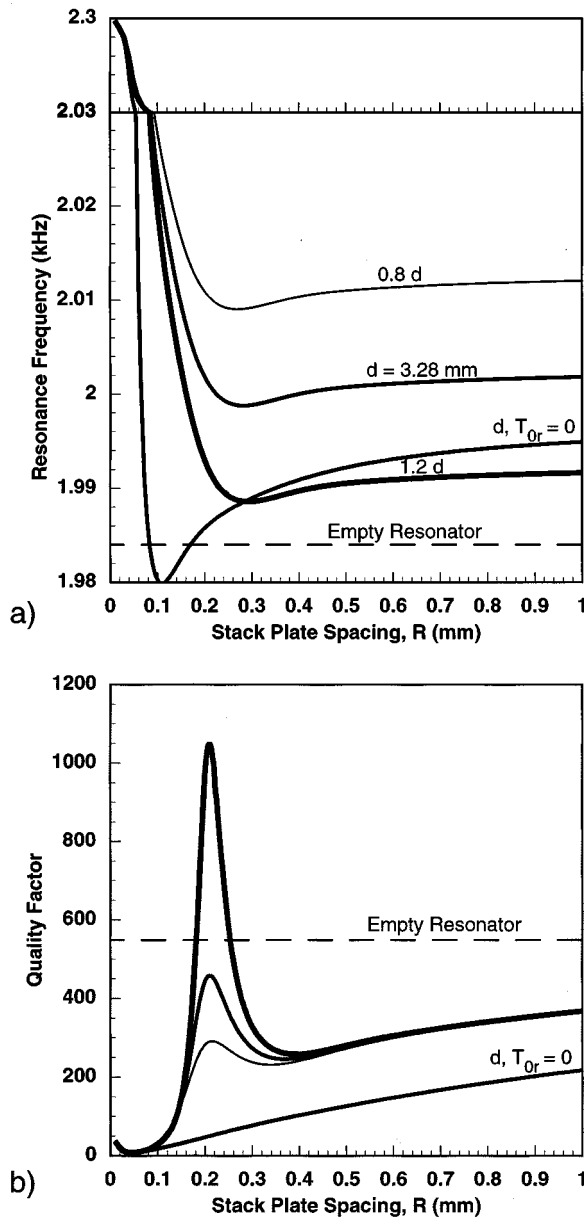


FIG. 5. (a) Resonance frequency and (b) quality factor of a radial wave prime mover below the onset of oscillation, as a function of stack and heat exchanger plate spacing R . The light, medium, and heavy weight curves labeled in (a) as $0.8d$, $d=3.28$ mm, and $1.2d$ all are for $T_{0z}=26.6$ K/mm. The medium weight curves in (a) and (b) labeled d , $T_{0r}=0$, are for no temperature gradient on the stack of length d , and the entire resonator at the ambient temperature. The dashed lines are for a resonator with no stack or heat exchangers.

on the same temperature as the stack (thermoacoustic drive ceases) and viscous losses increase.

The bending-up of the resonance frequency curves in Fig. 5(a) for decreasing $\lambda_T = \sqrt{2}R/\delta_\kappa$ has previously been observed experimentally for a stack in a plane-wave resonator where the ambient gas pressure and hence δ_κ was varied, though no explanation of the effect was given.⁴ Note that the frequency bends up for larger stack plate spacing as the hot end temperature increases. This can be explained in part by noting that $\delta_\kappa \propto (\kappa/\rho_0)^{1/2}$ increases with increasing temperature. Hence as the hot end temperature increases, λ_T decreases and the resonance frequency can bend up for larger R

than when no stack temperature gradient is present.

Close examination of Fig. 5(a) and (b) shows that the peak in Q for a particular plate spacing occurs in the vicinity of rapid variation of the resonance frequency. It is unfortunate that the peak in Q does not correspond to the relative minimum of resonance frequency. If it did, slight variations in any of the parameters, such as ambient temperature and pressure, would cause only small changes of the resonance frequency. It should be noted that a similar dependence for Q and resonance frequency were obtained for the plane-wave geometry, and that this geometry can also be used to increase the Q of these resonators for photoacoustic spectroscopy. It also should be noted that in practice, the Q can be increased reliably and controllably by at least a factor of 100 larger than the Q on an empty resonator.¹⁷

II. COMPARISON OF RADIAL AND PLANE-WAVE REFRIGERATORS USING THE SHORT STACK APPROXIMATION

The short stack approximation^{1,3,4} is given and used to compare some basic properties of radial and plane-wave engines. Basic assumptions are discussed in Refs. 1, 3, and 4. The stack temperature gradient is the constant $T_{0r}^{(\infty)}$ in the short stack approximation [see the discussion below Eq. (10)].

Pressure, particle velocity, and particle displacement amplitudes between the stack end and the resonator wall are taken to be the standing-wave forms

$$P_1(r) = P_1(0)J_0(k_0r), \quad (14a)$$

$$P_1(z) = P_1(0)\cos(k_0z), \quad (14b)$$

$$v_s(r) = \frac{P_1(0)}{\Omega\rho_0c} J_1(k_0r), \quad (15a)$$

$$v_s(z) = \frac{P_1(0)}{\Omega\rho_0c} \sin(k_0z), \quad (15b)$$

$$\xi_s(\phi) = \frac{v_s(\phi)}{\omega}, \quad (16)$$

where Eqs. (14a) and (15a) [Eqs. (14b) and (15b)] refer to the radial (plane) wave geometry. The acoustic propagation constant in the empty tube is $k_0 = \omega_0/c$ and ω_0 is the resonance frequency, Ω is stack porosity, and ϕ refers to either phase k_0r or k_0z . Use of Eqs. (14)–(16) in Eq. (50) of Ref. 3 yields

$$\begin{aligned} \bar{Q}_2(\phi) = & -\frac{\Omega A_{\text{res}} P_1(\phi) v_s(\phi)}{2} \beta T_0 \frac{\text{Im}[F^*(\lambda_T) F(\lambda)]}{(1+N_{\text{pr}})|F(\lambda)|^2} \\ & - \frac{\rho_0 c_p \Omega A_{\text{res}} v_s(\phi)}{2} \frac{\text{Im}\{F^*(\lambda_T) + N_{\text{pr}} F(\lambda)\}}{(1-N_{\text{pr}}^2)|F(\lambda)|^2} \\ & \times \xi_s(\phi) T_{0\phi}, \end{aligned} \quad (17)$$

where $T_{0\phi} = T_{0r}$ and $T_{0\phi} = T_{0z}$ are the constant temperature gradient for radial and plane-wave geometry, respectively. The first term in Eq. (17) is the time-averaged heat flow due to compression of the gas and can be exploited to construct acoustic refrigerators.¹ This heat flows in the stack toward

the nearest pressure antinode, and thus heat is transported from the cold to the hot end of the stack. Gas displaced to a region with different stack wall temperature results in heat transfer given by the second term of Eq. (17).¹ This heat always flows from the hot to cold end of the stack and is independent of β , the coefficient of thermal expansion. The stack acts as a refrigerator when the magnitude of the first term is larger than the magnitude of the second and the signs of these two terms are different. The second term of Eq. (17) thus reduces the cooling capacity of the refrigerator. For a prime mover, the magnitude of the second term in Eq. (17) is greater than the magnitude of the first term, so net heat is transported from hot to cold.

The work done in the stack is computed by use of the impedance translation theorem.³ Denote by $V_G = A_{\text{res}} \Omega d$ the ambient volume of gas in the stack. The work flow to first order in $k_0 d$ can be shown to have the same form as for the plane-wave geometry,^{3,4,18}

$$\begin{aligned} \bar{W}_2(\phi) = & \omega \frac{V_G P_1^2(\phi)}{2 \rho_0 c^2} (\gamma - 1) \text{Im} F^*(\lambda_T) \\ & + \omega \frac{\rho_0 V_G v_s^2(\phi)}{2} \frac{\text{Im} F^*(\lambda)}{|F(\lambda)|^2} \\ & + \frac{V_G P_1(\phi) v_s(\phi)}{2} \beta T_0 \phi \frac{\text{Im}\{F^*(\lambda_T)/F^*(\lambda)\}}{1 - N_{\text{pr}}}. \end{aligned} \quad (18)$$

The first and second terms, always >0 , are dissipation of potential and kinetic energy per unit time due to thermal and viscous effects. The third term is acoustic power produced or absorbed by the stack due to the ambient temperature gradient, and makes possible use of a thermoacoustic engine as a sound source. The stack will produce sound when the last term has a sign different than the first two terms, and a magnitude greater than the sum of these terms.

The resonator area at the stack is $A_{\text{res}} = 2\pi r h$ ($A_{\text{res}} = \pi a^2$) for radial (plane) wave geometry. Referring to Eq. (18), potential energy dissipation is proportional to $\{A_{\text{res}} P_1^2(\phi)\}$, kinetic energy dissipation is proportional to $\{A_{\text{res}} v_s^2(\phi)\}$, while thermoacoustic gain is proportional to $\{A_{\text{res}} P_1(\phi) v_s(\phi)\}$. These quantities are shown in Fig. 6(a) for plane and Fig. 6(b) for radial geometry. Note the high symmetry in Fig. 6(a), and lack thereof in Fig. 6(b) for the radial geometry. Referring to Fig. 2(a) and (b) and Fig. 6(a) and (b), one would like to place the stack at the locations of maxima for thermoacoustic gain; however, KE loss (which is usually more severe than PE loss) can be significantly reduced by placing the stack closer to pressure antinodes at the price of a slightly smaller thermoacoustic gain. Gain and losses $\rightarrow 0$ as $r \rightarrow 0$ for the radial geometry in Fig. 6(b) due to the dependence on A_{res} .

The assumptions necessary to compare radial and plane geometry refrigerators are given here. The same resonator will be used for both geometries in the comparison though the stack configuration will be as shown in Fig. 2(a) [Fig. 2(b)] for the radial (plane) geometry. Resonator aspect ratio a/h is determined by the condition that plane and radial stacks operate in resonators with the same eigenfrequency (a

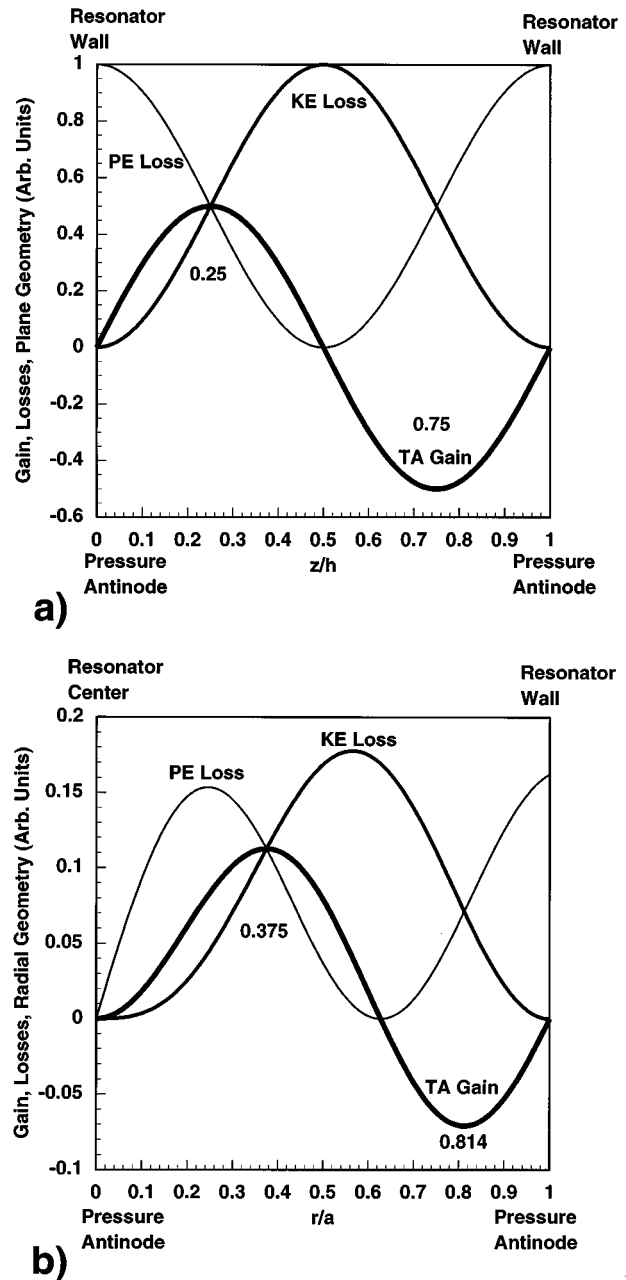


FIG. 6. Stack thermoacoustic gain, and losses of kinetic and potential energy, as a function of stack position in (a) a plane-wave resonator and (b) a radial wave resonator. Numbers on the graphs indicate positions of relative extrema of thermoacoustic gain.

condition likely to be avoided in practice). The conditions for determining plane and radial propagation numbers are $k_0 h = \pi$ and $k_0 a = 3.832$. Thus the resonator aspect ratio is $a/h = 3.832/\pi$. The working fluids are helium or a mixture of 60% helium and 40% argon so the assumed Prandtl numbers are $N_{\text{pr}} = 2/3$ or $N_{\text{pr}} = 0.392$, respectively. Ideal gas relations are used for other gas properties such as coefficient of thermal expansion and ratio of specific heats. The dimensionless thermal disturbance number $\lambda_T = (\rho_0 c_p \omega / \kappa)^{1/2} R$ is used to characterize the dynamic thermal interaction between fluid and solid, where R is the stack plate spacing. The maximum potential energy density¹ (which is half the stored overall energy density) in each resonator is assumed to be equal in

both cases, and is used to normalize the acoustic pressure using the relation $(1/V)\int P_1(\phi)^2 dV=1$. Here V is the resonator volume, and it is assumed that even when a short stack is present the pressure relations, Eqs. (14a) and (14b), are valid throughout the resonator. The normalization of radial (plane) geometry is $P_1(0)=2.483(\sqrt{2})$.

A nondimensional temperature gradient was previously⁴ helpful in the analysis of prime mover performance, and will also be used here. It is given by

$$\tau \equiv \frac{\beta \Delta T_0}{2k_0 d} \quad (19)$$

where d is the stack length, and $\Delta T_0=(T_{0z}d)$ for radial and plane geometries [see the discussion below Eq. (10)] is the ambient temperature difference between stack ends and can be positive or negative. The stack location is specified by the phase $\phi(r)=k_0 r$ [$\phi(z)=k_0 z$] for radial (plane) geometry. By combining the expression for A_{res} with the expressions above which define the resonator dimensions, one obtains $k_0^2 A_{\text{res}}=2\pi^2 \phi(r)$ ($k_0^2 A_{\text{res}}=3.832^2 \pi$) for radial (plane) geometry. The dimensionless forms of plate spacing λ_T , stack location ϕ , and stack temperature gradient τ are an example of similitude as applied in thermoacoustics.¹⁹

Refrigerators, cryocoolers, and air conditioners are usually designed for a given cooling temperature and cooling capacity. The coefficient of performance, COP , is the ratio of cooling power or capacity to the input power necessary to operate the refrigerator, and is usually also specified as a design criteria. The Carnot COP will be denoted as COP_c and is the highest COP possible for a given temperature span. A refrigerator designed solely for high cooling capacity will likely have a low COP , so often a trade-off between high cooling capacity and high COP must be accepted. Some design choices for thermoacoustic refrigerators are the working fluid and its ambient pressure, resonator size, sound source, heat exchangers capacity, stack geometry and material of construction, stack length and its location in the standing wave, and resonator mode (plane or radial) to use. With such a large list of design criteria and possible design configurations to consider, the challenge of comparing radial and plane-wave geometry thermoacoustic heat pumps appears at first to be daunting. Granted, no single set of criteria covers all aspects of refrigerator design. However, some design exploration using a reasonable set of system equations helps to build our intuition.

As an aid for determining how to compare radial and plane-wave acoustic refrigerators, consider the simple example developed by Swift¹ for his purpose of illuminating basic acoustic refrigerator properties. The example assumes an inviscid gas ($N_{\text{pr}}=0$) and the boundary layer approxima-

TABLE I. Optimized refrigerator parameters for helium as working fluid.

Quantity	Radial Inner	Plane	Radial outer
	$\Omega=70\%$ ($\Omega=50\%$)	$\Omega=70\%$ ($\Omega=50\%$)	$\Omega=70\%$ ($\Omega=50\%$)
λ_T	4.062 (4.150)	3.858 (3.900)	3.828 (3.871)
$\frac{r}{a}$ or $\frac{z}{h}$	0.220 (0.196)	0.096 (0.075)	0.928 (0.943)
τ	-0.168 (-0.134)	-0.266 (-0.243)	0.281 (0.256)
$\frac{\tau}{\tau_{\text{max}}}$	0.382 (0.371)	0.408 (0.403)	0.411 (0.406)
$\bar{Q}_2(\phi)$	18.50 (15.49)	14.60 (11.71)	10.68 (8.69)
$\frac{COP}{COP_c}$	0.162 (0.126)	0.244 (0.228)	0.254 (0.237)
C_1	2.988 (1.955)	3.560 (2.665)	2.715 (2.062)

tion for the thermal interaction of gas and stack. Heat flow in this example (using our notation) is

$$\bar{Q}_2(\phi) = -(A_{\text{res}}/\sqrt{2}\lambda_T)\beta T_0 P_1(\phi) \nu_s(\phi)(1-\Gamma),$$

where $\Gamma=T_{0\phi}/T_{0\phi,c}$ is the ratio of the actual stack temperature gradient to the critical temperature gradient given in Eqs. (1a) and (1b) for plane and radial geometries. Coefficient of performance is $COP=\Gamma COP_c$. For refrigerators, $0<\Gamma<1$. Immediately appreciate that to increase COP/COP_c , $\Gamma\approx 1$ is desirable. However, the cooling capacity of the refrigerator $\bar{Q}_2(\phi)\rightarrow 0$ as $\Gamma\rightarrow 1$. An acoustic refrigerator with a large COP is likely to have a low cooling capacity.

Our purpose here is to compare radial and plane-wave acoustic refrigerators, and not, for example, to decide on the best working fluid. To this end a useful quantity, the coefficient of compromise, C_m , is defined as

$$C_m \equiv \left(\frac{COP}{COP_c}\right)^m |\bar{Q}_2(\phi)| \quad (m\geq 0), \quad (20)$$

where different values of m can be used to choose a desired compromise between COP and cooling capacity. For example, C_1 refers to refrigerator design where coefficient of performance and cooling capacity are similarly emphasized, and C_5 has coefficient of performance emphasized considerably more than cooling capacity. The next task is to show how to calculate C_m for radial and plane-wave refrigerators to within a common factor.

The coefficient of performance is $COP=\bar{Q}_2(\phi)/\bar{W}_2(\phi)$. Note that $COP_c=T_C/\Delta T_0$ where T_C is the stack cold end temperature and $\Delta T_0=(T_H-T_C)$ is the temperature difference of the stack ends. Using the definition of τ in Eq. (19), the thermodynamic identity $\beta^2 T_0 c^2=(\gamma-1)/c_p$, and Eqs. (17) and (18) for heat and work flows, gives

$$\frac{COP}{COP_c} = \frac{-2\tau \left(\frac{J_0(\phi)J_1(\phi)}{\Omega} \frac{\text{Im}\{F^*(\lambda_T)F^*(\lambda)\}}{(1+N_{\text{pr}})|F(\lambda)|^2} + \frac{2J_1^2(\phi)}{\Omega^2} \frac{1}{\gamma-1} \frac{\text{Im}\{F^*(\lambda_T)+N_{\text{pr}}F(\lambda)\}}{(1-N_{\text{pr}}^2)|F(\lambda)|^2} \right)}{(\gamma-1)J_0^2(\phi)\text{Im}\{F^*(\lambda_T)\} + \frac{J_1^2(\phi)}{\Omega^2} \frac{\text{Im}\{F^*(\lambda)\}}{|F(\lambda)|^2} + 2\tau \frac{J_0(\phi)J_1(\phi)}{\Omega} \frac{\text{Im}\{F^*(\lambda_T)/F^*(\lambda)\}}{1-N_{\text{pr}}}} \quad (21)$$

for radial wave refrigerators. The plane-wave refrigerator COP/COP_c is also given by Eq. (21) with the replacements $J_0(\phi) \rightarrow \cos(\phi)$ and $J_1(\phi) \rightarrow \sin(\phi)$. The stack length d can be calculated using $k_0 d = (\beta T_0) / (2|\tau| COP_c)$.

Heat flow $\bar{Q}_2(\phi)$ is given in a different form from Eq. (17) to show how it is calculated in Eq. (20) to obtain C_m . The rewritten expression for cooling capacity for radial wave geometry is

$$\begin{aligned} \bar{Q}_2(\phi) = & \frac{\Omega k_0^2 A_{\text{res}} P_1(0)^2 \beta T_0}{[2\rho_0 c k_0^2]} \\ & \times \left(\frac{J_0(\phi) J_1(\phi)}{\Omega} \frac{\text{Im}[F^*(\lambda_T) F^*(\lambda)]}{(1 + N_{\text{pr}}) |F(\lambda)|^2} \right. \\ & \left. + \frac{2J_1^2(\phi)}{\Omega^2} \frac{\tau}{\gamma - 1} \frac{\text{Im}\{F^*(\lambda_T) + N_{\text{pr}} F(\lambda)\}}{(1 - N_{\text{pr}}^2) |F(\lambda)|^2} \right). \end{aligned} \quad (22)$$

The plane-wave result is also given by Eq. (22) with the replacements $J_0(\phi) \rightarrow \cos(\phi)$ and $J_1(\phi) \rightarrow \sin(\phi)$. Since use is made of the same working fluid and k_0 in the comparison of radial and plane geometries the quantity $[2\rho_0 c k_0^2]$ is common to both plane and radial refrigerators, so for simplicity, cooling capacities discussed below were computed using $[2\rho_0 c k_0^2] = 1$. It has already been shown how to calculate all of the other parameters in Eq. (22).

Heat flow in Eq. (22) vanishes for a sufficiently large dimensionless temperature gradient defined as τ_{max} . Evaluating the nontrivial solution for $\bar{Q}_2(\phi) \rightarrow 0$ yields

$$\begin{aligned} \tau_{\text{max}} = & -\frac{1 - N_{\text{pr}}}{2} \frac{P_1(\phi)}{\rho_0 c v_s(\phi)} (\gamma - 1) \\ & \times \frac{\text{Im}[F^*(\lambda_T) F^*(\lambda)]}{\text{Im}\{F^*(\lambda_T) + N_{\text{pr}} F(\lambda)\}}. \end{aligned} \quad (23)$$

The quantity τ_{max} is useful for comparison with values of τ and is analogous to the mean critical temperature gradient in Eq. (1). However, even for $\tau > \tau_{\text{max}}$, the thermoacoustic engine is not necessarily acting as a prime mover.¹ There exists a range of τ values such that $\tau_{\text{max}} < \tau < \tau_{\text{pm}}$ where the engine is not a refrigerator or prime mover, where τ_{pm} is the minimal temperature gradient necessary for the prime mover to operate.¹

Comparison of radial and plane-wave refrigerators now turns to the mathematical and computational side. We define the best radial or plane-wave refrigerator as the one which has the highest C_m . Following specification of the working fluid's γ , β , and N_{pr} , and the stack porosity Ω , values of λ_T , ϕ , and τ can be floated around using numerical techniques until they land on a specific unique set of critical values that produce a maximum of C_m . Cooling capacity and COP/COP_c can be obtained using these critical values of λ_T , ϕ , and τ . Keep in mind that stack plate spacing can be determined from λ_T , stack location in the standing wave from ϕ , and both stack length d and refrigerator temperature difference from the combination of τ and the desired COP_c .

Table I shows the results of C_1 optimization, where cooling capacity and COP/COP_c are taken to be equally im-

portant, for helium as the working fluid. Computations were performed for stack porosities of $\Omega = 0.7$ and $\Omega = 0.5$. As Ω decreases, particle velocity in the stack must increase to ensure that volume velocity is continuous at the stack-resonator section interface. As noted in Table I, radial inner has a higher value of λ_T than the others because larger values of λ_T correspond to less overall KE loss²⁰ and thus the stack position $r/a = \phi/(k_0 a)$ can be closer to the peak of thermoacoustic gain in Fig. 6(b). Since heat flow is proportional to r for the radial stacks, the radial inner stack, which is at smaller r , must be pushed as far as possible away from the origin to achieve reasonable heat flow, though at a cost of increased viscous loss. The critical λ_T for the radial inner case is larger than the others to reduce these viscous losses. Decreasing stack porosity increases the optimal λ_T , again to circumvent KE loss.²⁰ Stack position is reported in Table I as r/a for radial wave and z/h for plane-wave geometries. Note that the optimal stack positions are well away from the locations of maximum thermoacoustic gain in Fig. 6(a) and (b) due to the need for reducing KE dissipation. The ratios of optimal τ to the value of τ_{max} for which refrigeration ceases are also shown in Table I. The ordering from smallest to largest (τ/τ_{max}) occurs for radial inner, then plane, to radial outer. Note that τ_{max} in Eq. (23) is proportional to the standing-wave temperature gradient in Eq. (1) when the inviscid limit $N_{\text{pr}} \rightarrow 0$, $F(\lambda) \rightarrow 1$ is applied to Eq. (23). The ordering for largest to smallest magnitude of the standing-wave temperature gradient in Eq. (1) and Fig. 1 is radial inner, then plane, to radial outer, which is the ordering from smallest to largest (τ/τ_{max}). The stack with highest cooling capacity is radial inner. Note that decreasing stack porosity decreases cooling capacity and COP/COP_c in all cases. Also note that the radial outer has the highest COP/COP_c . Finally, the plane stacks have the largest C_1 .

Having seen that small stack porosity compounds viscous losses, it is increased to $\Omega = 0.9$ to reduce these losses. Viscous losses can be reduced further by going to a molar mixture of 60% He/40% Ar for which the Prandtl number is taken to be $N_{\text{pr}} = 0.392$. Also investigated are compromise refrigerators where cooling capacity is emphasized more than COP/COP_c [$m = 0.5$ in Eq. (20)], where they are on equal footing ($m = 1$), and at a number of cases where COP/COP_c is emphasized more than cooling capacity ($m = 1.5 - 4$ at steps of 0.5). The findings are that plane-wave refrigerators have higher C_m when $1 \leq m \leq 5$, indicating that they perhaps are the best overall choice when COP/COP_c must be emphasized more than cooling capacity, and that the radial wave inner stack has higher C_m when $m = 0.5$, indicating that they perhaps are the best choice when cooling capacity is emphasized more than COP/COP_c . Figure 7 clearly shows that increasing COP/COP_c decreases cooling capacity for all of these acoustic refrigerators. Note that the radial outer case has the highest COP/COP_c , though the plane case is very similar. The cooling capacity of the radial inner case is highest for small m , but the plane case is larger for large m . Figure 8 shows that λ_T increases as m increases, which implies that wider stack plate spacing reduces viscous losses and thus increases COP/COP_c , but reduces cooling capacity since the optimal value for cooling capacity is $\lambda_T = 3.2$.³

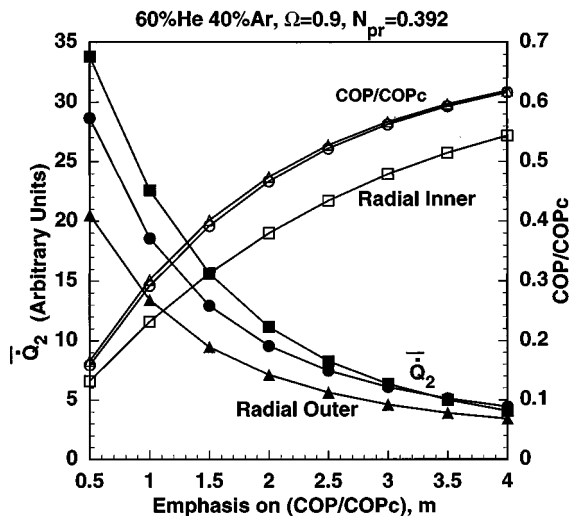


FIG. 7. Cooling capacities and coefficient of performance ratios as a function of the emphasis, m , on coefficient of performance. Calculation points are shown by the symbols and the lines connect these points for viewing ease. Solid symbols are cooling capacity, squares refer to radial inner stacks, triangles to radial outer, and circles to plane stacks. COP/COP_c nearly overlap for plane and radial outer.

Keeping in mind the ideal stack positions for obtaining high thermoacoustic gain and low KE losses due to gas viscosity as shown in Fig. 6(a) and (b), Fig. 9 shows that as COP/COP_c is emphasized increasingly more than cooling capacity, the stack location migrates away from thermoacoustic gain and toward low KE loss.

For fixed COP_c , Fig. 10 shows that the stack temperature gradient increases as COP/COP_c is increasingly emphasized, or, equivalently, stack plate height $k_0 d = (\beta T_0) / (2|\tau|COP_c)$ decreases. The influence of the thermoacoustic term [the third term of Eq. (20), which is opposite in sign to the first two terms] for work flow increases for larger $|\tau|$ which has the effect of increasing COP/COP_c . Figure 11 bolsters this observation since $\tau/\tau_{max} \rightarrow 1$ when COP/COP_c is emphasized much more than cooling capacity. Note that the

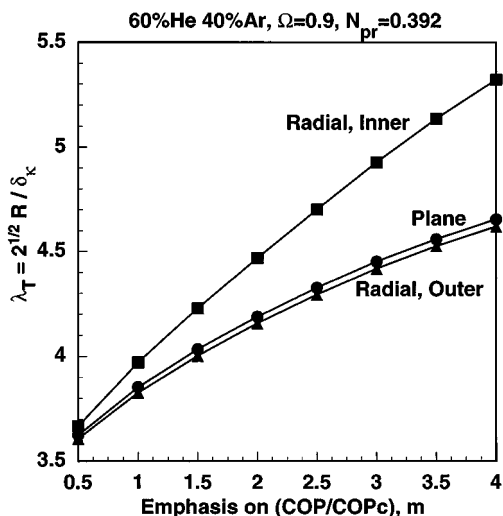


FIG. 8. Thermal disturbance numbers λ_T as a function of the emphasis, m , on coefficient of performance. Symbols are the same as in Fig. 7.

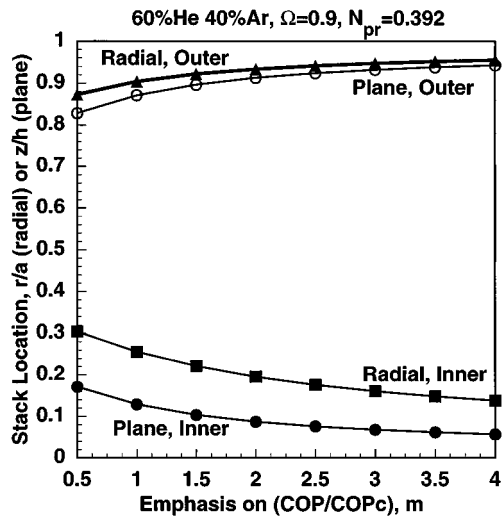


FIG. 9. Stack locations as a function of the emphasis, m , on coefficient of performance. Symbols are the same as in Fig. 7.

radial inner case has the lowest τ/τ_{max} which is consistent with this case producing high cooling capacities and low COP/COP_c . Radial outer and plane cases have very similar τ/τ_{max} ratios.

III. CONCLUSION

A general linear framework was developed for analyzing radial wave thermoacoustic engines. Pressure and specific acoustic impedance translation equations were developed for the various thermoacoustic elements, and the stack enthalpy flow can be expressed in terms of these variables. Theory for the use of thermoacoustic engines to enhance the signal-to-noise ratio of photoacoustic spectrometers was developed. In this example it was noted that the dependence of resonance frequency on stack plate spacing can be very different, depending on whether a temperature gradient is applied across the stack. The thermoacoustic enhanced photoacoustic spec-

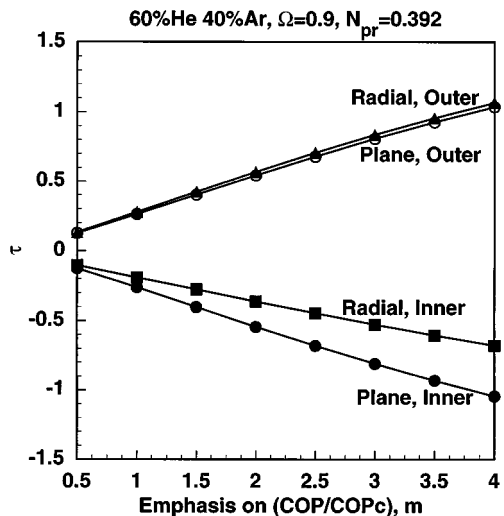


FIG. 10. Nondimensional temperature gradients τ as a function of the emphasis, m , on coefficient of performance. Symbols are the same as in Fig. 7.

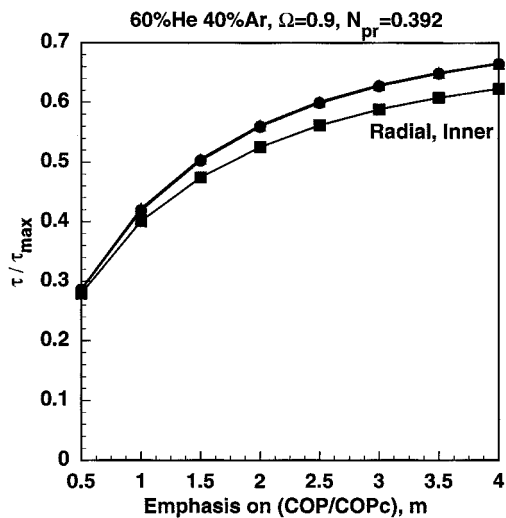


FIG. 11. Ratios of the nondimensional temperature gradient τ to the maximum possible value for refrigeration, τ_{\max} , as a function of the emphasis, m , on coefficient of performance. Symbols are the same as in Fig. 7. The radial outer and plane results nearly overlap.

trometer was likened to an analog amplifier with amplification Q , bandwidth f_0/Q , and discrimination against acoustic noise (signal-to-noise ratio) $Q^{1/2}$, where f_0 is the resonance frequency and Q is the quality factor.

The short stack approximation was given for radial and plane-wave geometries, and was used to compare the performance of refrigerators constructed using these stacks. Refrigerator performance was evaluated using the weighted product of cooling capacity and coefficient of performance as a measure of capability. Independent parameters for refrigerators were stack plate spacing, stack location in the standing wave, and stack length. Results of the comparison are that engines in the plane-wave geometry are better overall refrigerators when maximizing both cooling capacity and coefficient of performance, though radial stacks placed near the resonator center can have higher cooling capacities and radial stacks near the resonator wall have slightly higher coefficients of performance. It was noted that to improve thermoacoustic engine performance, the viscous losses associated with the square of particle velocity need to be lowered without sacrificing too much desirable thermoacoustic gain associated with the product of particle velocity and acoustic pressure. Finally, the radial analysis and intuition developed here is qualitatively applicable to nominally plane-wave resonators where the resonator radius increases along the axis.

ACKNOWLEDGMENTS

This work was supported by the Office of Naval Research. W. P. Arnott and H. Moosmüller are also supported

for the photoacoustic application by the Environmental Protection Agency, Office of Exploratory Research. The authors thank Henry E. Bass for his suggestions and contributions to this research. Jeffery R. Olson made helpful suggestions for the refrigerator comparisons.

- ¹G. W. Swift, "Thermoacoustic engines," *J. Acoust. Soc. Am.* **84**, 1145–1180 (1988).
- ²N. Rott, "Thermoacoustics," *Adv. Appl. Mech.* **20**, 135–175 (1980).
- ³W. P. Arnott, H. E. Bass, and R. Raspet, "General formulation of thermoacoustics for stacks having arbitrarily shaped pore cross sections," *J. Acoust. Soc. Am.* **90**, 3228–3237 (1991).
- ⁴W. P. Arnott, J. R. Belcher, R. Raspet, and H. E. Bass, "Stability analysis of a helium-filled thermoacoustic engine," *J. Acoust. Soc. Am.* **96**, 370–375 (1994).
- ⁵W. P. Arnott, H. Moosmüller, R. Purcell, J. Lightfoot, R. Raspet, and H. E. Bass, "Thermoacoustic enhancement and control of the quality factor in a resonant photoacoustic cell for measurement of light absorption by aerosols and gases," *J. Acoust. Soc. Am.* **95**, 2811(A) (1994).
- ⁶A. D. Pierce, *Acoustics: An Introduction to Its Physical Principles and Applications* (American Institute of Physics, New York, 1989).
- ⁷W. C. Chew, *Waves and Fields in Inhomogeneous Media* (Van Nostrand Reinhold, New York, 1990), pp. 161–182.
- ⁸D. K. Holger, "The attenuation of sound propagating through a radial diffuser with absorptive walls," *J. Sound Vib.* **79**, 1–9 (1981).
- ⁹Comparison of the notation used here and in Ref. 3 with that used in Ref. 1 is discussed in the paragraph following Eq. (48) in Ref. 3.
- ¹⁰A. A. Atchley, H. E. Bass, T. J. Hoffer, and H. T. Lin, "Study of a thermoacoustic prime mover below onset of self-oscillation," *J. Acoust. Soc. Am.* **91**, 734–743 (1992).
- ¹¹A. A. Atchley and F. M. Kuo, "Stability curves for a thermoacoustic prime mover," *J. Acoust. Soc. Am.* **95**, 1401–1404 (1994).
- ¹²A. A. Atchley, "Standing wave analysis of a thermoacoustic prime mover below onset of self-oscillation," *J. Acoust. Soc. Am.* **92**, 2907–2914 (1992).
- ¹³A. A. Atchley, "Analysis of the initial buildup of oscillations in a thermoacoustic prime mover," *J. Acoust. Soc. Am.* **95**, 1661–1664 (1994).
- ¹⁴P. M. Morse and K. U. Ingard, *Theoretical Acoustics* (Princeton U.P., Princeton, NJ, 1968), pp. 519–522.
- ¹⁵K. M. Adams, "Real-time *in situ* measurements of atmospheric optical absorption in the visible via photoacoustic spectroscopy. 1: Evaluation of photoacoustic cells," *Appl. Opt.* **27**, 4052–4056 (1988).
- ¹⁶R. Gerlach and N. M. Amer, "Brewster window and windowless resonant spectrophones for intracavity operation," *Appl. Phys.* **23**, 319–326.
- ¹⁷W. P. Arnott, H. Moosmüller, R. E. Abbott, and M. D. Ossofsky, "Thermoacoustic enhancement of photoacoustic spectroscopy: Theory and measurements of the signal to noise ratio," *Rev. Sci. Instrum.* **66**, 4827–4833 (1995).
- ¹⁸W. P. Arnott, R. Raspet, and H. E. Bass, "Thermoacoustic engines," in *Proceedings of the 1991 IEEE Ultrasonics Symposium* (IEEE, New York, 1991), Vol. 2, pp. 995–1003. The last term of Eq. (6) should be $\text{Im}\{F^*(\lambda_T)/F^*(\lambda)\}$.
- ¹⁹J. R. Olson and G. W. Swift, "Similitude in thermoacoustics," *J. Acoust. Soc. Am.* **95**, 1405–1412 (1994).
- ²⁰Kinetic energy loss in Eq. (20) is proportional to $\text{Im} F^*(\lambda)$. As shown in Fig. 5 of Ref. 3, $|\text{Im} F^*(\lambda)| \rightarrow 0$ as $\lambda \rightarrow \infty$. Hence KE dissipation diminishes as λ increases beyond $\lambda \approx 3.2$. However, the desired thermoacoustic gain is roughly proportional to $\text{Im} F^*(\lambda_T)$, and the largest value of $\text{Im} F^*(\lambda_T)$ occurs for $\lambda_T \approx 3.2$. Keep in mind that $\lambda_T = N_{pr}^{1/2} \lambda$, so usually $\lambda_T < \lambda$. Hence the choice of optimal λ_T is balanced by a trade-off between the optimal value $\lambda_T = 3.2$ for thermoacoustic gain and the desire for low KE dissipation by gas viscosity which occurs for $\lambda \gg 3.2$.